THE ASTROPHYSICAL JOURNAL, 241: 552–560, 1980 October 15

X-RAY MEASUREMENTS OF THE MASS OF M87

D. FABRICANT, M. LECAR, AND P. GORENSTEIN
Center for Astrophysics, Harvard College Observatory and Smithsonian Astrophysical Observatory
Received 1980 February 6; accepted 1980 April 16

ABSTRACT

Soft X-ray images of the M87 region have been obtained using the imaging proportional counter aboard the *Einstein* Observatory. We have mapped the 0.7–3.0 keV surface brightness of M87 to a radial distance exceeding 50′ where it falls 2.5 orders of magnitude below its peak value. The temperature profile of the hot (~2.5 keV) gas responsible for the X-ray emission has been determined from the X-ray spectral data. The gas temperature is approximately constant between radii of 6′ and 20′, but decreases at radii less than 6′. Beyond 20′, a negative temperature gradient is excluded.

Because this gas responds to the gravitational potential of M87, the X-ray observations may be used to measure the radial mass distribution in M87. The well-supported hypothesis of hydrostatic equilibrium relates this mass distribution directly to the density and temperature profiles of the gas. As suggested by previous authors, we find that M87 possesses a dark halo. We estimate that the mass of this halo lies between $1.7\times10^{13}\mathfrak{M}_\odot$ and $4.0\times10^{13}\mathfrak{M}_\odot$ within a radius of 50′ or 230 kpc.

Subject headings: galaxies: individual — galaxies: structure — X-rays: sources

I. INTRODUCTION

The determination of the mass of galaxies is a fundamental goal of astrophysical research. Optical and 21 cm radio measurements have provided indications that the major component of the mass of galaxies is in the form of a dark halo extending far beyond the optically bright central region (Ostriker, Peebles, and Yahil 1974; Einasto, Kaasik, and Saar 1974). In particular, photometric and photographic studies of the giant elliptical galaxy, M87, have shown that it possesses a faint, extensive, optical corona, implying that its mass may be underestimated by conventional optical methods (Arp and Bertola 1969; de Vaucouleurs and Nieto 1978). In the case of M87, the mass distribution may be determined quantitatively from X-ray observations in a straightforward manner. With new data from the *Einstein Observatory* providing much more complete coverage of the X-ray emitting gas associated with M87, the incomplete picture built up from a number of earlier X-ray observations (Lea *et al.* 1973; Malina, Lampton, and Bowyer 1976; Gorenstein *et al.* 1977) can be clarified. The purpose of this paper is to describe the large scale structure of the X-ray source surrounding M87 and the massive dark halo the new observations require. We use the ~1′ resolution imaging proportional counter (IPC) data obtained by the *Einstein Observatory*. A later paper will describe in detail the few arcsec resolution data covering the centermost regions of the X-ray source, obtained using the high resolution imaging detector.

The most significant result of the present analysis is the refinement of our understanding of the mass distribution in M87. Previous experimenters have established that the preponderance of the X-ray emission surrounding M87 is thermal emission from a plasma at a temperature between 2 and 3 keV (Mushotzky *et al.* 1978; Fabricant *et al.* 1978; Lea *et al.* 1979). The fact that the surface brightness profile of an X-ray emitting gas is useful as a probe of the gravitational potential that contains it has been pointed out by a number of authors including Lea (1975), Gull and Northover (1975), Cavaliere and Fusco-Femiano (1976), and Bahcall and Sarazin (1977*a*, *b*), among others. In particular, Bahcall and Sarazin (1977*a*, *b*) considered polytropic models for the X-ray emission from the M87 region and concluded that if the X-ray emitting gas were gravitationally bound to M87, M87's mass would exceed $10^{13}\mathfrak{M}_\odot$. Most of this mass would lie in an optically dark halo extending to a radius of ~100 kpc. Based on fits of similar models to X-ray scans of the M87 region, Mathews (1978) came to the same general conclusion, but suggested that the mass of M87 might exceed $10^{14}\mathfrak{M}_\odot$ within a radius of ~300 kpc. However, the assumption inherent in the polytropic (or isothermal) models considered by these authors that the gas temperature falls with radius (or remains constant) disagrees with the present X-ray observations, which strongly suggest a positive temperature gradient. The vastly increased statistical precision and coverage of the data available from the *Einstein Observatory* provide the most substantial evidence found to date for a

dark halo surrounding an elliptical galaxy, and allow an accurate determination of the halo mass.

In § II, we describe the quantitative observational results concerning the density distribution and temperature gradient of the hot gas surrounding M87. In § III, we interpret these results within the context of a simple model in which the gas is confined in hydrostatic equilibrium in the gravitational potential of M87. In so doing, we calculate the total mass of M87 out to a radial distance of 50′. Within a radius of 50′, uncertainties in the temperature profile of the gas are, at present, the limitation in the determination of the dark halo's mass. Beyond 50′ from M87, it becomes increasingly difficult to separate emission associated with M87 from the background of the Virgo cluster.

II. RESULTS-THE HOT GAS DISTRIBUTION

The 60′×60′ field of view of the imaging proportional counter aboard the *Einstein Observatory* was centered on M87 beginning on 1978 December 20, 9:21 UT. This detector is sensitive to soft X-rays in the 0.2 to 4.5 keV energy range and attains a spatial resolution of ∼1.′5×1.′5 (FWHM) at 1 keV. The instrument is described in detail by Giacconi *et al.* (1979). Approximately 200,000 photons were detected in a 14,000 second observation. Because the emission surrounding M87 extends beyond the field of view of the detector, data from a 25,000 second pointing 63′ south and 25′ east of M87 were also analyzed allowing azimuthally incomplete coverage to a radial distance exceeding 100′ from M87. As previous reports had suggested (Davison 1978; Lawrence 1979; Forman *et al.* 1979), there is evidence for weak, very diffuse emission associated with the Virgo cluster at large, in addition to the much more intense extended emission of M87. The spectrum of the Virgo cluster source is considerably harder than that of M87.

A 0.7–3.0 keV contour plot of the data from the first pointing is shown in Figure 1. Background from charged particles has been subtracted, and the data have been corrected for unequal exposure due to vignetting by the telescope optics; both these corrections are small. The data have been smoothed with a 2′ (FWHM) Gaussian weighting function to eliminate statistical jitter. The emission in the central region (20′ diameter) plotted is circularly symmetric on a scale of a few arcmin. A region of obstruction by the detector window support structure and uncertainties in the uniformity of both the soft X-ray background and the Virgo cluster emission prevent a firm statement on the precise degree of symmetry at larger radii.

However, assuming that radial symmetry continues at larger radii, we have binned the data in concentric annuli about the centroid of the X-ray emission to obtain a radial surface brightness profile. The centroid of the X-ray emission is coincident with the optical

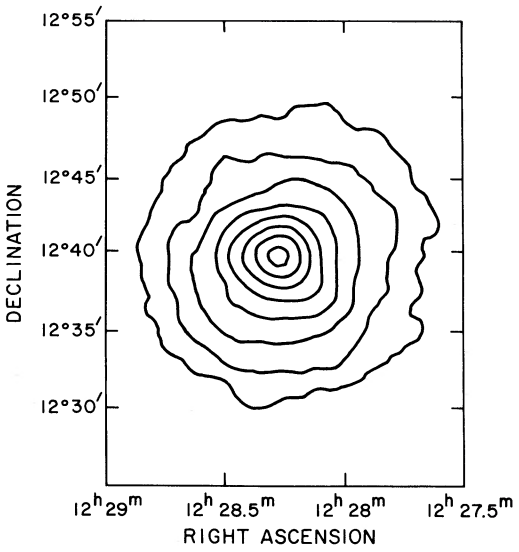

FIG. 1.—A 0.7–3.0 keV contour plot of M87. The data have been smoothed with a 2′ (FWHM) Gaussian weighting function. The contour levels are separated by a factor of 1.5 in surface brightness.

nucleus of M87 within the present 40″ positional uncertainty of the imaging proportional counter. The surface brightness profile in units of X-ray counts s^{-1} $arcmin^{-2}$ keV^{-1} in the 0.7–3.0 keV energy band is plotted in Figure 2. The points at radial distances exceeding 30′ are taken from the pointing to the southeast of M87, where an approximately 60 degree azimuthal coverage is available. Data between radii of 17′ and 22′ are not shown because of the large systematic errors associated with the correction for the obscuration of the window support structure located in this region. Counts due to the Virgo cluster source, as well as charged particle events and the X-ray background, have been subtracted from the data before plotting. In addition, these data are corrected for the off-axis vignetting of the telescope. The charged particle and X-ray background have been determined from several long pointings at high galactic latitude, and the Virgo cluster background has been taken from the offset pointing position to the southeast of M87. The estimated uncertainties due to systematic errors associated with background subtraction are included in the error bars shown in Figure 2.

The 0.7–3.0 keV surface brightness of M87 falls to a level equal to that of the Virgo cluster diffuse source in the same energy band at a radial distance between 50′ and 55′, and falls to less than 10% of this level between 70′ and 75′. Making use of a preliminary analysis of the high resolution imager data, we have found that less than 5% of the counts at radii less than 3′ are due to a compact central source, and a negligible amount beyond that. Thus, the preponderance of the X-ray emission surrounding M87 is extended emission from hot gas.

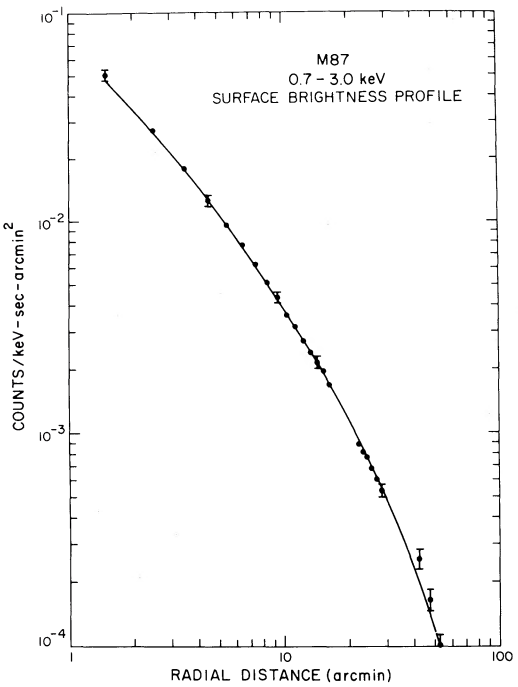

FIG. 2.—The 0.7 to 3.0 keV surface bright profile of M87. Background from the Virgo cluster intracluster gas, charged particles, and the diffuse X-ray background has been subtracted. Correction for the vignetting of the X-ray telescope off-axis has been made. The solid line is a fit to the data (from eqs. [1] and [2]).

Another measurement of great physical interest is the temperature profile of this gas. It has been established that the X-ray spectrum of this gas is rich in lines (principally from iron L shell transitions) perhaps most convincingly by the two high resolution spectral instruments on board the *Einstein Observatory*. Unfortunately, neither of these instruments, which consist of a solid state and a crystal spectrometer, are sensitive enough to trace the temperature profile as the surface brightness falls much below the peak levels. The imaging proportional counter has only modest energy resolution, amounting to $\sim$100% at 1.5 keV. Thus, changes in spectra due to temperature and abundance cannot be differentiated because at temperatures near 2 keV, a temperature decrease and an abundance increase both produce more intense emission from the iron lines that dominate the spectrum near 1 keV. Recognizing that our ability to measure absolute temperatures is limited by uncertainties in the iron abundance, by possible uncertainties in the theory describing radiation from a hot plasma containing heavy elements, and by systematic uncertainties in the calibration of the imaging proportional counter, we have chosen to concentrate on the limited objective of searching for a temperature gradient in the spectral data as it is observed in projection along the line of sight. In the temperature analysis, we have assumed that no significant abundance gradient is present.

For this purpose, the spectral data were binned in six radial bands about the centroid of the X-ray emission, 0′–3′, 3′–6′, 6′–9′, 9′–12′, 12′–17′, and 23′–27′. Nine pulse height bins were used for the spectral fits, spanning the range 0.2–3.0 keV. The data in the region 17′–23′ were excluded due to the obscuration by the detector window support structure mentioned previously, and those beyond 27′ were excluded because of the large systematic uncertainties associated with the background subtraction in this region. The background from the Virgo intracluster gas has not been subtracted from the spectral data. The background contamination from this source is less than 5% in the 12′–17′ band, and less than 15% in the 23′–27′ band. The X-ray and particle background and its systematic uncertainty (estimated to be 20% of the level subtracted) were determined by studying the background variations in a number of long exposures on high galactic latitude fields containing no strong sources. These errors were added in quadrature to the statistical errors. Model spectra calculated using the code of Raymond and Smith (an updated version of Raymond and Smith 1977) for an equilibrium plasma were convolved with the detector response and compared to the data using the χ^2 test. Throughout the spectral fitting, the iron abundance was held fixed at 4.0×10^{-5} relative to hydrogen. Absorption by interstellar matter in our galaxy was included. However, due to the residual systematic errors in the calibration of the instrument's spectral response coupled with the very high statistical precision of the M87 data, the minimum χ^2 values found exceeded 4 per degree of freedom. Assuming that these systematic errors may be represented as efficiency corrections for each raw pulse height channel, we evaluated these correction factors using data in one of the radial bands.

To force an acceptable fit, the errors associated with the data in the 6′–9′ radial band were increased to 10%. The best fitting model (now with reduced $\chi^2\approx1$) had a temperature of 2.5 keV and an absorption corresponding to a hydrogen column of 2.5×10^{20} atoms cm^{-2}. Both of these values are consistent with previous measurements (Mushotzky *et al.* 1978; Fabricant *et al.* 1978; Lea *et al.* 1979). Efficiency corrections for each pulse height channel were calculated by dividing the predicted counts for the best-fit model by the data. The data in the remaining radial rings were corrected with these efficiency factors and fit in the normal fashion with the statistical errors and background subtraction errors discussed previously.

Naturally, this method of forcing an acceptable fit sacrifices accuracy in the determination of the absolute gas temperature, but it should have a much smaller effect upon the detection of a temperature gradient. The results of the spectral fits are shown in Figure 3.

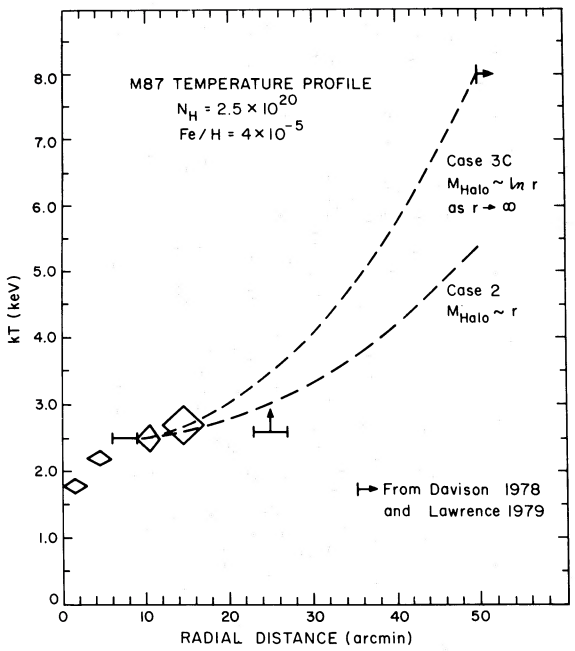

FIG. 3.—The temperature profile of M87 derived by fits to the spectral data. N_H has been fixed at 2.5×10^{20} and the ratio of iron to hydrogen abundance in the gas has been fixed at 4.0×10^{-5} for these fits. A limit derived from Davison (1978) and Lawrence (1979) is also plotted. The dotted lines correspond to the temperature gradients expected for two possible halo radial mass dependences. The data in the 6′–9′ band has been used to correct pulse height bin efficiencies (see text).

The hydrogen column was held fixed at 2.5×10^{20} cm^{-2} and the iron abundance in the gas surrounding M87 was fixed at 4.0×10^{-5} relative to hydrogen, so only the normalization and temperature were fitted. The error bars shown in Figure 3 are the 90% confidence (statistical) limits evaluated using the results of Lampton, Margon, and Bowyer (1976), and correspond to the limits at which the χ^2 of the fits increase by 4.6 from the best fitting model. The χ^2 per degree of freedom for the best fitting models were less than 1 in all cases once the channel efficiency corrections were applied, with the exception of the two centermost radial bins. Here acceptable fits were found only if the energy range was restricted to 0.7 to 3.0 keV. Two factors may explain this phenomenon. The spatial response function of the detector broadens as the detected pulse height drops, causing the central radial bins of a sharply peaked distribution to be deficient in low pulse height events which is what we observe. In addition, since there are indications of a temperature gradient in the central region of M87 both in our own data and in that from other instruments aboard the *Einstein Observatory*, it is not surprising that a single temperature model is a poor description of the spectrum as observed in projection along the line of sight. A complex spectrum in the central region (6′ diameter) of M87's X-ray emission has been reported by Mushotzky *et al.* (1980) based on the preliminary analysis of spectral data from the solid state spectrometer on board the *Einstein Observatory*. Canizares *et al.* (1979) have detected the O VIII line from M87 with a focal plane crystal spectrometer. This line is characteristic of plasmas with temperatures below 10^7K, which is less than the mean M87 gas temperature. In any event, we may extract with confidence one result from Figure 3; the allowable temperature gradient in the region 6′–17′ is quite small, but possibly positive with increasing radius at large radii. Since we observe a weighted average of the spectra through the projection of the gas distribution, the gas temperature must remain approximately constant at radii some what beyond 17′. A negative gradient is inconsistent with the spectral results.

The spectral data have been used to calculate the incident flux and intrinsic luminosity of M87 in the 0.2–3.0 keV energy band. The incident flux, corrected for interstellar absorption in our galaxy, is $4.5 \times 10^{\times 10}$ ergs cm^{-2} s^{-1}, within a projected radius of 28′ of M87. If azimuthal symmetry is assumed, the flux within a projected radius of 50′ is 5.5×10^{-10} ergs cm^{-2} s^{-1}. At the distance of M87, 15.7 Mpc (Mould, Aaronson, and Huchra 1980), these correspond to luminosities in the same energy band of 1.3×10^{43} ergs s^{-1}, and 1.6×10^{43} ergs s^{-1}, respectively.

In order to calculate the density distribution of the gas surrounding M87, the observed surface brightness distribution must be deprojected. This inversion is dependent on the temperature profile of the gas, but fortunately not strongly so at temperatures above 2.5 keV, as shown in Figure 4. This plot gives the relative power detected in the 0.7–3.0 keV energy band of the IPC from a fixed volume of gas (enriched with heavy elements) as its temperature varies between 1.5 and 6 keV. A computer program was written to accept specified azimuthally symmetric density and temperature profiles and compute the resultant surface brightness profile in the energy band of the imaging proportional counter. Appropriate weighting factors were used to account for interstellar absorption and the instrument's energy dependent sensitivity. Simulations were carried out to test the sensitivity of the surface brightness profile to temperature gradients. A density profile of the form $\rho(r)\alpha(1+r^2/12.25)^{-0.68}$ was selected because it is a convenient analytic function that produces a surface brightness similar to that observed in the range of 5′–40′ if the gas is assumed to be isothermal. Using the computer program, the surface brightness distribution was calculated for the case in which kT varies between 1 keV at the center to 6 keV at 60′. This temperature gradient is more extreme than the observed one, at least in the range of 6′–20′ (Fig. 3). This surface brightness profile was then deprojected numerically (solving the Abel integral equation) neglecting the temperature gradient, and assuming that the emission is

proportional to the square of the density as would only be exactly true for the isothermal case. With the exception of the regions where the temperature falls well below 2 keV, the resulting density profile is quite similar to the one assumed in calculating the surface brightness profile. These two distributions agree to within 30% beyond 4′. The logarithmic derivatives of the density profiles, which are used in § III, agree within 25% at radii greater than 5′. Thus, the uncertainty in the measurement of the temperature gradient in M87 does not result in a large systematic error in the density profile calculated using the surface brightness data.

An analytically convenient function of the form:

$$I(r)=\frac{I_0}{(1+br^2+cr^4+dr^6)^n}, \quad (1)$$

where r is measured in arcmin, was fit to the surface brightness profile. Although this function has no particular physical significance, it provides an excellent description of the data (with a set of coefficients $b=1.009$, $c=2.386\times10^{-3}$, $d=1.845\times10^{-7}$ and $n=0.68$), passing within the error bars of the data except for one point at 42′. An acceptable representation for the surface brightness distribution motivated by theory is not presently available. The principal shortcoming of the polytropic models that have been extensively discussed in the literature is that they fail to consider the effect of the intracluster gas. The above function was then inverted numerically under the assumption of isothermality to find the density profile. The resultant density distribution is well represented by the expression:

$$\rho(r)=\frac{\rho_0}{(1+b'r^2+c'r^4+d'r^6)^n}, \quad (2)$$

where r is measured in arcmin and $b'=9.724\times10^{-1}$, $c'=3.810\times10^{-3}$, $d'=2.753\times10^{-8}$, and $n=0.59$. The surface brightness profile predicted from this density distribution, assuming an isothermal gas, is the solid line in Figure 2. The electron density normalization, ρ_0, has been found to be 5.4×10^{-2} cm^{-3} by requiring the luminosity predicted within a projected radius of 28′ of the center of M87 to agree with the measured value of 4.5×10^{-10} ergs cm^{-2} s^{-1} in the 0.2–3.0 keV energy band. The electron density distribution is shown in Figure 5. The corresponding mass density normalization is 1.0×10^{-25} g cm^{-3}. Table 1 contains the integrated mass of gas within radii of 10′, 20′, 30′, 40′, and 50′ from the center of M87. The logarithmic derivative of the density profile is plotted in Figure 6.

The densities predicted by this formula are an upper limit to the actual densities at radii less than ~6′ because the temperature in this region is known to be lower than that assumed. As mentioned previously, the power radiated by a plasma in the energy band of the imaging proportional counter increases as the temperature decreases in this temperature regime. Furthermore, the ~5% contribution to the data at radii less than 3′ due to the compact source near the center of M87 has not been subtracted.

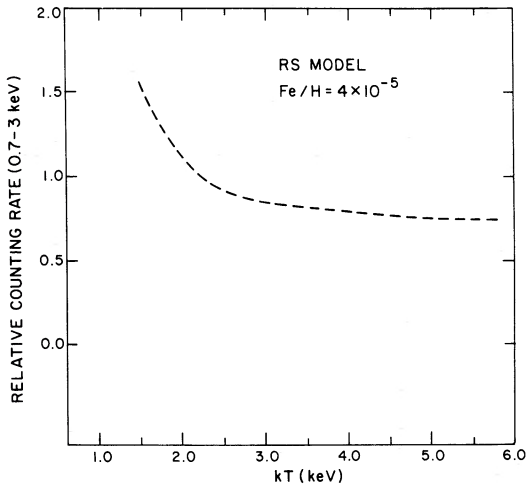

FIG. 4.—The relative number of counts detected in the 0.7–3.0 keV energy band of the IPC from a fixed volume of gas (enriched with heavy elements) as its temperature is varied between 1.5 and 6 keV.

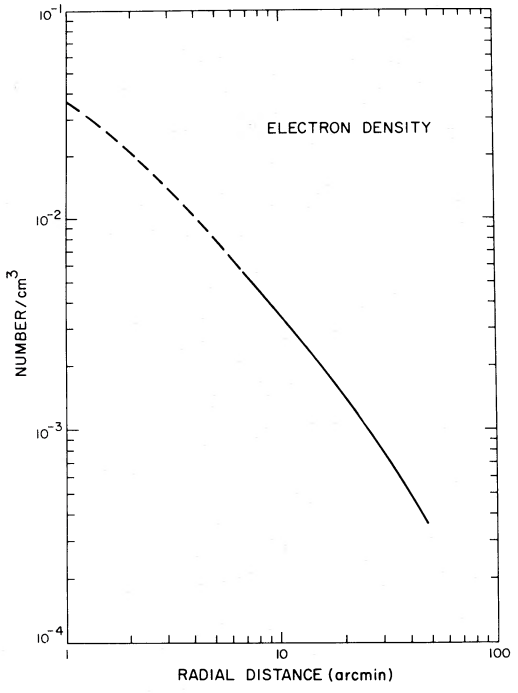

FIG. 5.—The electron density profile derived from the surface brightness data under the assumption of isothermality. The dotted portion of the curve represents an upper limit to the density.

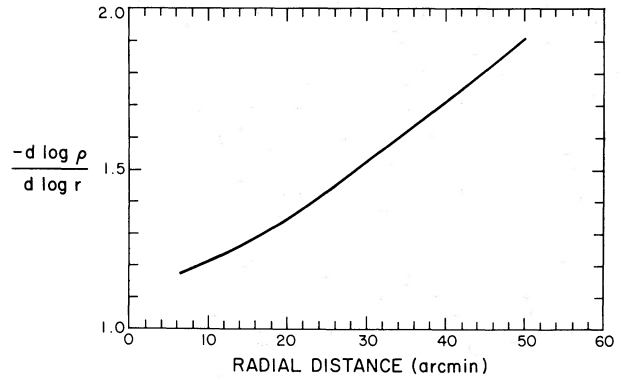

FIG. 6.—The logarithmic derivative of the density distribution plotted in Fig. 5.

III. DISCUSSION-THE MASS DISTRIBUTION IN M87

We base our analysis on the hypothesis that the X-ray emitting gas is in hydrostatic equilibrium with the gravitational field of M87. We believe that this is the case for three reasons. The strongest argument for hydrostatic equilibrium is that the cooling time of the gas is everywhere much longer than the dynamical, or freefall, time. Table 2 compares these two quantities at several radii. The small radiative losses could be equalized by the gravitational energy gained at infall rates less than ~ 10 km s^{-1}. Two observational results support the hydrostatic equilibrium hypothesis. The gas temperature does not increase inward as would be expected if the gas were settling or expanding adiabatically. Second, the density profile of the bulk of the X-ray emitting gas is not as steep ($\rho[r] \approx r^{-2}$) as would be expected for freely expanding or falling gas.

The fact that X-ray emitting gas has remained associated with M87, illuminating the gravitational potential in which it is captured, is probably the result of its special situation in the Virgo cluster. The line-of-sight velocity of recession for M87 is within errors the same as the mean of the values for the Virgo cluster (Tammann 1972). If the velocity component transverse to the line of sight is also small, stripping of M87's gas will have been minimal. The fact that M87 is the most luminous X-ray source associated with a galaxy in the Virgo Cluster by two orders of magnitude may thus not be the result of an inherent peculiarity but a consequence of its environment.

TABLE 1

MASS OF GAS IN M87 ($D = 15.7$ Mpc)

Radius (Arcmin)	Radius (kpc)	Solar Masses of Gas
10.....	46	6.5×10^{10}
20.....	91	2.2×10^{11}
30.....	137	4.5×10^{11}
40.....	183	7.2×10^{11}
50.....	228	1.0×10^{12}

The equation that an ideal gas in hydrostatic equilibrium must obey is easily derived by combining the (spherically symmetric) condition of hydrostatic equilibrium with the ideal gas law:

$$\frac{dP_{\rm gas}}{dr} = \frac{-G\mathfrak{M}_*(r)\rho_{\rm gas}}{r^2} \tag{3}$$

where $P_{\rm gas}$ is the gas pressure, $\rho_{\rm gas}$ is the density, G is the gravitational constant, and $\mathfrak{M}_*(r)$ is the mass of M87 interior to the radius r.

$$P_{\rm gas} = \frac{\rho_{\rm gas} K T_{\rm gas}}{\mu \mathfrak{M}_{\rm H}} \tag{4}$$

where μ is the mean molecular weight (taken to be 0.6), and $\mathfrak{M}_{\rm H}$ is the mass of hydrogen atom. We use these to obtain:

$$\frac{KT_{\rm gas}}{\mu\mathfrak{M}_{\rm H}}\left(\frac{d\rho_{\rm gas}}{\rho_{\rm gas}} + \frac{dT_{\rm gas}}{T_{\rm gas}}\right) = \frac{-G\mathfrak{M}_*(r)}{r^2}dr, \tag{5}$$

which may be rewritten as:

$$-\frac{KT_{\rm gas}}{G\mu\mathfrak{M}_{\rm H}}\left(\frac{d\log\rho_{\rm gas}}{d\log r} + \frac{d\log T_{\rm gas}}{d\log r}\right)r = \mathfrak{M}_*(r) \tag{6}$$

If $T_{\rm gas}$ is a constant, this simplifies to:

$$-\frac{KT_{\rm gas}}{G\mu\mathfrak{M}_{\rm H}}\left(\frac{d\log\rho_{\rm gas}}{d\log r}\right)r = \mathfrak{M}_*(r). \tag{7}$$

Equation (7) is a good approximation between radii of 6′ and 20′, where both the temperature and the

TABLE 2

COOLING AND FREE-FALL TIMES OF THE GAS SURROUNDING M87

Radial Distance (arcmin)	Radial Distance (kpc)	Radiative Cooling Time $T_{\rm cool}$(years)	Freefall Time $T_{\rm freefall}$(years)	Ratio of $T_{\rm cool}/T_{\rm freefall}$
5.....	23	2.5×10^{9}	3.3×10^{7}	76
10.....	46	6.4×10^{9}	6.8×10^{7}	94
20.....	91	1.5×10^{10}	1.5×10^{8}	100
30.....	140	2.7×10^{10}	2.1×10^{8}	130

logarithmic derivative of the density are observed to be nearly constant. Thus, substituting $-d\log\rho/d\log r\approx 1.24$, $T\approx 2.5$ keV, we have:

$$\mathfrak{M}_{\rm total}\approx 1.2\times 10^{13}\mathfrak{M}_{\odot}\left(\frac{r}{100\,\rm kpc}\right), \tag{8}$$

where 100 kpc$\approx$21′.9. This is very similar to the prediction of Bahcall and Sarazin (1977*b*) in the isothermal limit. Thus, hydrostatic equilibrium immediately leads to total masses for M87 that far outweigh the mass of the visible matter, which in turn implies the existence of a dark halo. If this halo can be characterized as an isothermal gas sphere with an isotropic velocity dispersion, $C_{\rm H}^2$, the pressure in the halo is given by $P_{\rm H}(r)=1/3\rho_{\rm H}(r)C_{\rm H}^2$. Substituting this into the equation of hydrostatic equilibrium for the halo (identical to eq. [3] for the gas), and using equation (7), we obtain:

$$C_{\rm H}^2=\frac{3}{2}\frac{G\mathfrak{M}_*}{r}=\frac{3}{2}\frac{kT}{\mu\mathfrak{M}_{\rm H}}\left(\frac{-d\log\rho_{\rm gas}}{d\log r}\right). \tag{9}$$

Substituting the same quantities used for equation (8), we find $C_{\rm H}\approx 850$ km s^{-1}. Although $C_{\rm H}^2$ is a useful number for reference, most models of halo formation predict a strong radial bias in the velocity dispersion (Gott 1977). This contrasts with the velocity dispersion of the luminous matter which ranges between 350 and 600 km s^{-1} (Sargent *et al.* 1978).

Because $-d\log\rho/d\log r$ continues to increase at large radii (see Fig. 6), the assumption that the X-ray emitting gas is everywhere isothermal leads to the somewhat implausible conclusion from equation (7) that the rate of increase of the halo mass rises with radius. If the gas temperature increases with radius, equation (6) must be used. In this case, the positive temperature gradient offsets the negative density gradient, and the halo mass increases more slowly with radius than in the isothermal situation. Such a temperature gradient is allowed by the spectral data, and in fact, is expected on physical grounds. As mentioned previously, the Virgo cluster is known to contain a hot ($\sim$8 keV) gas (Davison 1978; Lawrence 1979) with a density of $\sim 5\times 10^{-4}$ cm^{-3} (Forman *et al.* 1979). This cluster gas will help confine the gas surrounding M87 when the pressures of the two become comparable. Since thermal conduction will act to force the temperatures of the M87 gas and the cluster gas to equalize in the boundary region, it seems quite plausible that the temperature of the M87 gas rises at large radii. The density profile plotted in Figure 6 suggests that this boundary layer lies in the region of 50′–60′, or 230–270 kpc.

a) Effect of a Temperature Gradient Upon the Mass Determination

As mentioned previously, the poorly determined radial temperature dependence of the gas beyond 20′ from M87 is the major systematic uncertainty in the measurement of the halo mass at radial distances less than 50′. In § IV, we examine the effect a temperature gradient has upon the determination of the halo mass in order to understand the limits of this uncertainty at present and to provide a basis for the interpretation of future, more precise spectral data. Equation (6) may be integrated to calculate the temperature profile that corresponds to any choice of radial halo mass dependence, making use of the observed gas density distribution. In general, the more positive the temperature gradient, the lower the halo mass implied by the X-ray observations. We have considered five different possibilities for these coupled pairs of temperature profiles and halo mass distributions. The simplest of these, which almost certainly over estimates the halo mass, is the isothermal case. We label this case 1 for reference. For case 2, the halo mass is assumed to increase linearly with radius throughout the observed region. Case 3 covers more extreme situations in which the halo density distribution steepens with increasing radius, and the halo mass increases more slowly than for case 2. For case 3, we have considered three specific possibilities, which are all of the general form

$$\mathfrak{M}_*(r)=\frac{2}{3}\frac{C_{\rm H}^2}{G}r\mu(r), \tag{10}$$

where $\mu(r)$ is a dimensionless expression that asymptotically modifies the radial mass dependence. The three subcases considered are:

case 3*a*

$$\mu(r)=\frac{\beta}{\beta-1+(r/r_0)},$$

where $\mathfrak{M}_*(r)\rightarrow$Constant and $\rho_{\rm H}(r)\alpha r^{-4}$ as $r\rightarrow\infty$; case 3*b*

$$\mu(r)=\frac{\beta}{\beta-1+(r/r_0)^{0.5}},$$

where $\mathfrak{M}_*(r)\alpha r^{0.5}$ and $\rho_{\rm H}(r)\alpha r^{-2.5}$ as $r\rightarrow\infty$; and case 3*c*

$$\mu(r)=\frac{\beta+\ln(r/r_0)}{\beta-1+(r/r_0)},$$

where $\mathfrak{M}_*(r)\alpha\ln(r)$ and $\rho_{\rm H}(r)\alpha r^{-3}$ as $r\rightarrow\infty$. In each case, r_0 was taken to be 7′, the point at which the integration of equation (6) to derive the temperature gradient was begun. At r_0, the quantity $d\log T/d\log r$ was assumed to be zero, and T, the gas temperature, was taken to be 2.5 keV. This radius was chosen because $d\log\rho/d\log r$ changes most slowly here, implying that the rate of change $d\log T/d\log r$ also is smallest here. Small errors in $d\log T/d\log r$ and the gas temperature at r_0 have little effect on the calculated

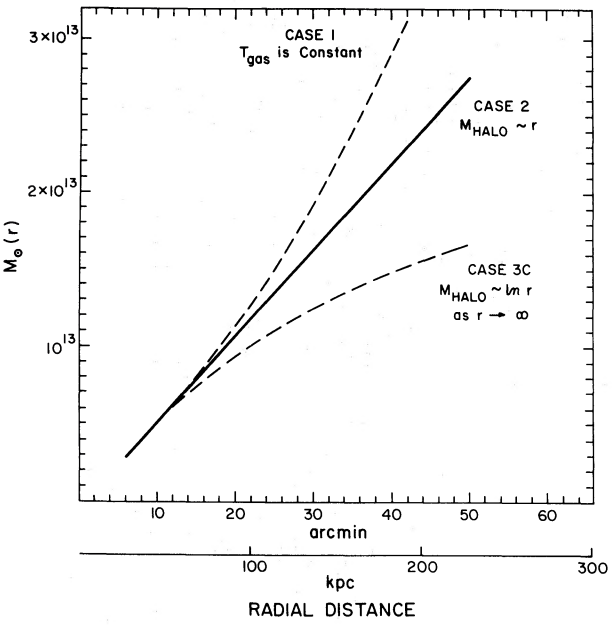

FIG. 7.—The radial mass dependence of M87, as derived in § III.

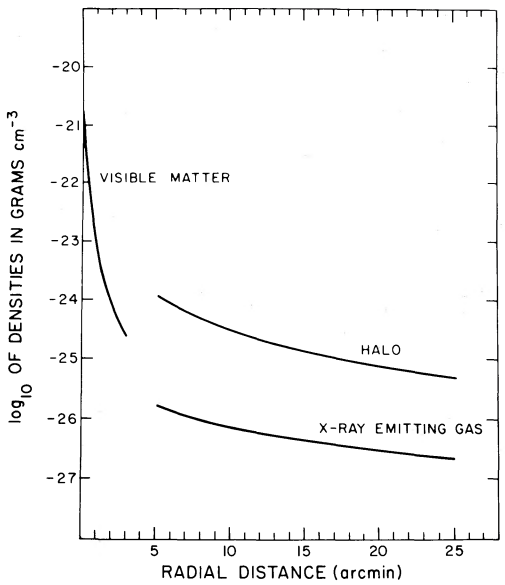

FIG. 8.—The approximate density profiles of the halo, X-ray emitting gas, and visible matter in M87. The visible density profile has been derived from data given in Sargent *et al.* (1978). The regions of high uncertainty are not plotted.

mass. With r_0 fixed, β was chosen so that the gas temperature just reaches 8 keV, the Virgo cluster gas temperature, at 50′ from M87 where the cluster emission begins to dominate. The gas temperature may in fact be well below 8 keV at 50′ from M87, but the extreme case considered here produces the steepest temperature gradient (and lowest mass) consistent with available measurements. All three of the forms 3*a*, 3*b*, and 3*c* produce similar results when constrained in the fashion described, but 3*c* gives slightly lower halo mass than 3*a* or 3*b*. For 3*c*, the lowest β allowed is 3.55. The resulting expressing provides a reasonable estimate of a lower limit to the halo mass, which is $1.7\times10^{13}\mathfrak{M}_\odot$ within a radius of 50′. The mass distributions predicted in cases 1, 2, and 3*c* are plotted in Figure 7. The corresponding temperature profiles are shown in Figure 3. Cases 1 and 3*c* may be reasonably expected to bracket the range of mass dependences allowed by the data.

IV. CONCLUSIONS

Based solely on the X-ray data and the well supported hypothesis of hydrostatic equilibrium, we have demonstrated that M87 has a dark halo whose extent is at least 50′ or 230 kpc. Within this radius, we estimate that the halo mass lies in the range of $1.7\times10^{13}\mathfrak{M}_\odot$–$4.0\times10^{13}\mathfrak{M}_\odot$. In contrast, the core radius of the visible matter in M87 is 10″ or 0.8 kpc. Figure 8 compares the density profiles of the halo, the X-ray emitting gas, and the density distribution deduced from visible light observations. The usefulness of the present data is limited beyond 50′ by uncertainties in the background from the Virgo cluster and the X-ray background. In any case, because M87's halo ceases to dominate the gravitational potential in the Virgo cluster at some distance from M87, the X-ray measurements are in principle unable to set an upper limit to the mass of M87. Present estimates of the density of intracluster gas within the Virgo cluster suggest that this distance is near 50′–60′ from M87. More refined spectral data will aid in the determination of the exact radial dependence of the mass distribution, which will be of interest in considerations of the halo formation. These measurements will require the next generation of X-ray instruments capable of simultaneous good spectral and spatial resolution.

The authors are pleased to acknowledge useful discussions with Andrew Fabian of the Institute of Astronomy and Paul Schecter, now at Kitt Peak National Observatory. We thank John Raymond of the Center for Astrophysics for providing us with a revised version of the Raymond and Smith code that calculates the X-ray emission from an optically thin plasma enriched with heavy elements.

REFERENCES

Arp, H., and Bertola, F. 1969, *Ap. J.* (*Letters*), **4**, 23.
Bahcall, J., and Sarazin, C. 1977*a*, *Ap. J.* (*Letters*), **213**, L99.
_____. 1977*b*, *Ap. J.*, **219**, 781.
Canizares, C., Clark, G., Markert, T., Berg, C., Smedira, M., Bardas, D., Schnopper, H., and Kalata, K. 1979, *Ap. J.* (*Letters*), **234**, L33.

Cavaliere, A., and Fusco-Femiano, R. 1976, *Astr. Ap.*, **49**, 137.
Davison, P. 1978, *M.N.R.A.S.*, **183**, 39P.
de Vaucouleurs, G., and Nieto, J. 1978, *Ap. J.*, **220**, 449.
Einasto, J., Kaasik, A., and Saar, E. 1974, *Nature*, **250**, 309.
Fabricant, D., Topka, K., Harnden, Jr., F. R., and Gorenstein, P. 1978, *Ap. J. (Letters)*, **226**, L107.
Forman, W., Schwarz, J., Jones, C., Liller, W., and Fabian, A. 1979, *Ap. J. (Letters)*, **234**, L27.
Giacconi, R., *et al.* 1979, *Ap. J.*, **230**, 540.
Gorenstein, P., Fabricant, D., Topka, K., Tucker, W., and Harnden, F. R., Jr. 1977, *Ap. J. (Letters)*, **216**, L95.
Gott, R. J., III. 1977, *Ann. Rev. Astron. Ap.*, **15**, 235.
Gull, S., and Northover, K. 1975, *M.N.R.A.S.*, **173**, 585.
Lampton, M., Margon, B., and Bowyer, S. 1976, *Ap. J.*, **208**, 177.
Lawrence, A. 1979, *M.N.R.A.S.*, **185**, 423.
Lea, S., Silk, J., Kellogg, E., and Murray, S. 1973, *Ap. J. (Letters)*, **184**, L105.
Lea, S. 1975, *Ap. Letters*, **16**, 141.
Lea, S., Mason, K., Reichert, G., Charles, P., and Riegler, G. 1979, *Ap. J. (Letters)*, **227**, L67.
Malina, R., Lampton, M., and Bowyer, S. 1976, *Ap. J.*, **209**, 678.
Mathews, W. 1978, *Ap. J.*, **219**, 413.
Mould, J., Aaronson, M., and Huchra, J. 1980, *Ap. J.*, submitted.
Mushotzky, R. *et al.* 1980, in preparation.
Mushotzky, R., Serlemitsos, P., Smith, B., Boldt, E., and Holt, S. 1978, *Ap. J.*, **225**, 21.
Ostriker, J., Peebles, P., and Yahil, A. 1974, *Ap. J. (Letters)*, **193**, L1.
Raymond, J., and Smith, B. 1977, *Ap. J. Suppl.*, **35**, 419.
Sargent, W., Young, P., Boksenberg, A., Shortridge, K., Lynds, C., and Hartwick, F. 1978, *Ap. J.*, **221**, 731.
Tammann, G. 1972, *Astr. Ap.*, **21**, 355.

DANIEL FABRICANT, PAUL GORENSTEIN, and MYRON LECAR: Harvard-Smithsonian Center for Astrophysics, 60 Garden Street, Cambridge, MA 02138